Fire Safety Journal 120 (2021) 103075

Contents lists available at ScienceDirect

Fire Safety Journal

journal homepage: http://www.elsevier.com/locate/firesaf

An experimental study of the behavior of 3D printed concrete at elevated temperatures

Antonio Cicione *, Jacques Kruger, Richard S. Walls, Gideon Van Zijl

Department of Civil Engineering, Stellenbosch University, Stellenbosch, 7600, South Africa

ARTICLE INFO

Keywords:
3D printing of concrete
Concrete in fire
Material thermal behavior
Interlayer bond strength

ABSTRACT

3D printing of concrete (3DPC) is an automated layer-wise construction technique that does not require temporary support, such as formwork, during the construction process. It facilitates the realization of geometrically complex objects at reduced construction time, and potentially cost, compared to conventional construction techniques. However, with technological advancements and new innovative construction methods, such as 3DPC, it is still crucial to understand their performance in fire. Although concrete structures generally have a good reputation for their behavior in fire, there is negligible literature available on the behavior of 3DPC at evaluated temperatures. It is with this backdrop that this paper conducts a preliminary investigation on the behavior of 3DPC at elevated temperatures by conducting an experimental study. Eight concrete samples, consisting of both 3DPC and conventionally casted concrete, were tested by exposing the samples to a high incident heat flux via radiant panels, along with an additional 15 samples to obtain ambient strength properties. It was found that 3DPC is less susceptible to thermo-hygral spalling as a result of higher permeability and porosity in the 3DPC specimens compared to normally casted concrete. However, the 3DPC samples delaminated between layers (thermo-mechanical) as a result of reduced flexural strength.

1. Introduction

Digital construction, an additive manufacturing technology emerging from the Fourth Industrial Revolution, presents significant potential to industrialize the construction industry. This layer-wise construction technique facilitates free-form construction of geometrically complex elements at reduced construction time and cost compared to conventional construction techniques [1]. Several projects have been completed using 3D printing of concrete (3DPC), among others a pre-stressed bridge in the Netherlands and a state-of-the-art office building in the United Arab Emirates. However, a current pertinent disadvantage of this technology is the inability to automatically include steel reinforcement in the construction process [2]. Also, a specific issue that currently attracts significant attention is the influence that the interlayer bond has on the mechanical properties of 3D printed concrete (3DPC) elements [3]. Recent studies show that up to a 36% reduction in flexural strength is obtained for 3D printed samples due to the effect of the interlayer bond [4]. With technological advancements and new innovative construction methods, such as 3DPC, it is important to understand their performance in fire. In general, concrete structures have a reputation for behaving well in fires [5]. When heated, the cement paste undergoes an endothermic reaction, thus reducing the rise in temperature of the fire exposed side. Since concrete has a low thermal conductivity and is non-combustible, it serves as good insulation that protects the reinforcing steel against heat. Although concrete in fire has been studied extensively by past researchers [6–9], there is negligible literature available on the behavior of 3DPC in fire, and it is important to answer the question: does the 3D printing process influence the fire resistance of samples? Numerous questions remain unanswered with regard to 3DPC in fire, with an obvious area of concern being the behavior of the interlayer bonding when heated. It is with the above mentioned in mind that the paper seeks to investigate the behavior of 3DPC at elevated temperatures. Typically, concrete mixes used for 3DPC have much higher strengths [10]. According to Buchanan and Abu [5], high strength concrete (e.g. 3DPC) is typically more susceptible to thermo-hygral spalling compared to normal concrete, because of higher compressive stresses and smaller free pore volume. Hence, the pores are typically filled with high pressure water vapour more rapidly, compared to normal weight concrete, and the low porosity results in slower diffusion of water vapour through the concrete. However, to limit the

* Corresponding author.
E-mail address: acicione@sun.ac.za (A. Cicione).

https://doi.org/10.1016/j.firesaf.2020.103075
Received 6 January 2020; Accepted 28 April 2020
Available online 4 May 2020

number of variables discussed in this paper only 3DPC mix designs are used, and not conventional mixes. Furthermore, in this work radiant panels are used to subject concrete samples to high heat fluxes, rather than testing samples under conventional standard fire furnace conditions. This is done to create thermal gradients in small samples such that the effect of thermal curvature and induced stresses can be more easily studied.

2. Interlayer bond behavior at ambient temperature

3DPC differs fundamentally from conventionally casted concrete techniques as it utilizes a pump to transport the material from a hopper to a nozzle for extrusion. High pressures are imparted on the concrete during pumping that result in microstructural breakdown of interparticle forces in thixotropic materials [11]. Consequently, some entrapped air escapes during the shearing of the material, resulting in a denser concrete after extrusion. Both porosity and density are important parameters that influence concrete behavior at elevated temperatures and are determined for the 3D printable material in the sections that follow. 3DPC elements comprise of multiple filament layers that are deposited in a layer-wise manner during the additive manufacturing process. The layers bond to one another to yield the desired 3DPC element. However, research indicates that the interlayer bonds reduce the tensile strength of 3D printed elements, resulting in quasi-homogenous elements. This behavior frequently occurs in 3D printing and is referred to as lack of fusion, with similarity to cold joint formation in conventional concrete construction terms. Typically, the flexural and tensile strength of 3DPC elements reduce as the time between deposition of successive filament layers increase, as depicted in Fig. 1. Van der Putten et al. [12] ascribe the decrease in strength to the loss of moisture in the filament layer. Sanjayan et al. [13] share similar sentiments. As the bottom layer becomes drier with increasing printing time gap (Fig. 1), it absorbs more water from the freshly deposited top filament layer, which causes air in the bottom layer to escape and become entrapped at the interface. However, in another study by the same authors, they found that increasing the surface roughness of filament layers has a greater impact than moisturizing the substrate [14]. Kruger et al. [10] found that, for a small printing time gap and thus minimal loss of surface moisture, enhancing thixotropy behavior of the printable material improves the interlayer bond strength. Many theories have been tested and much work is still required to fundamentally understand the processes responsible for the lack of fusion in 3DPC. The authors of this research postulate that the lack of fusion may largely be attributed to the increased porosity (including capillary porosity) at the interlayer positions, yielding mechanically weaker concrete.

3. Experimental setup

In order to best understand the complex behavior of 3DPC at elevated temperatures, the experimental setup was simplified to represent a one-dimensional heat conduction scenario. Eight samples were tested in total, where samples were subdivided into: (i) two 160 × 160 × 40 mm (L × H × W) samples of conventionally casted concrete, as depicted in Fig. 2, (ii) three 160 × 165 × 50 mm samples that were 3D printed as depicted in Fig. 3, and (iii) three 160 × 160 × 40 mm samples that were 3D printed and cut to have smooth edges with the same dimensions as the casted concrete, as depicted in Fig. 4.

In 3DPC structures, single layers are often printed, rather than multiple layers next to each other. These are connected to other layers in a truss-like manner, meaning that single lamina may be exposed to fire, and hence testing has been done in this manner. The 160 mm wide 3DPC samples were cut out of a 560 × 240 × 165 mm (L × W × H) rectangular printed section as depicted in Fig. 5. The maximum current nozzle size of the 3D printer at Stellenbosch University is 25 mm in diameter. Thus, it was necessary to over extrude, which consequently lead to less appealing aesthetics, in order to have a 40–50 mm wide sample, i.e. to perform four-point bending tests on the printed samples as discussed in a

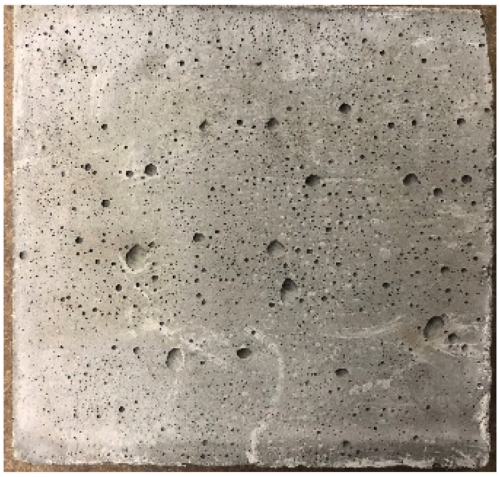

Fig. 2. Casted concrete sample.

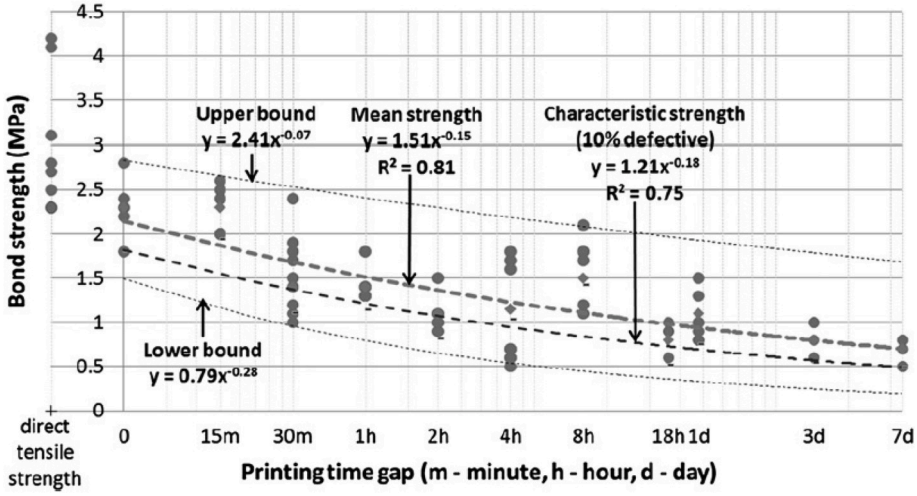

Fig. 1. Interlayer bond strength of 3D printed concrete samples for varying printing time gaps compared to the direct tensile strength of a reference sample (reworked from Ref. [4]).

Fig. 3. 3DPC sample.

Fig. 4. Cut 3DPC sample.

later section. Since, the focus of the paper is on the effect of elevated temperatures on 3DPC, the aesthetics were not prioritized, but rather practicality.

The samples were exposed to direct radiation of approximately 50–60 kW/m^2 via radiant panels acting perpendicular to the front face of the sample, as depicted in Fig. 6. The samples were heated until the thermocouples embedded in the middle of the samples reached a temperature of 300 °C. The sides of the samples were completely covered with ceramic blanket and the backside exposed to the environment in order to ensure one-dimensional heat transfer. The distance between the radiant panels and the test samples was approximately 50 mm.

It should be noted that the boundary layer (i.e. as a result of convection) established at both the surface of radiant panels and the water-cooled heat flux gauges (HFGs) are overlapping, meaning that the sample and the HFGs were exposed to some amount of convection (as opposed to only radiation). This would have resulted in a small error in the heat flux (HF) readings, since the HFGs are only calibrated for radiation, but had no effect on the measured front surface, inside and back surface temperatures. Ultimately the temperatures are the results of interest, with heat fluxes simply indicating the exposure.

3.1. Instrumentation layout

The instrumentation layout is depicted in Fig. 7. K-type thermocouples were used, connected to an Agilent 34980A data logger, and a 4-wire resistance temperature detector (RDT) was used as external reference temperature. The 3DPC samples had 12 thermocouples in total, with 4 thermocouples placed between printed layers, 4 thermocouples placed within the printed layers, and 2 thermocouples placed on the front and back of the sample surface, respectively. The normally casted concrete (NCC) samples were equipped with 8 thermocouples in total, with 4 thermocouples placed within the sample, 2 thermocouples placed on the front and back of the sample surface, respectively. The thermocouples placed in the middle of the samples were embedded by drilling a small hole (1.5 mm diameter) in order to fit the (1.5 mm) thermocouple inside. The holes were sealed with fire sealant to keep the thermocouples in place. The thermocouples placed on the face of the sample were fixed by drilling a hole that is half the diameter (0.75 mm) of the thermocouples (1.5 mm), sticking the tip of the thermocouple into the hole, adding a small amount of fire sealant (note that the sealant did not make contact with the tip of the thermocouple), and lastly covering exposed sealant with aluminum foil tape to avoid the radiation affecting thermocouple readings. Two HFGs were placed on the sides of the test samples, in gypsum board, spaced 35 mm from the edge of the sample to the center of the HFG and 80 mm from the bottom of the sample to the center of the HFG, as depicted in Fig. 6.

4. Materials and mixing

4.1. Concrete mix composition and grading

The 3D printable concrete mix ingredients and proportions used for this research are given in Table 1.

A low water to cement ratio of 0.45 is employed, thus resulting in a HPC. This allows for superplasticizer addition that improves thixotropy behavior, which is deemed ideal for 3DPC [11]. Typically, materials with higher water to cement ratios demonstrate less thixotropy behavior and consequently perform badly in 3DPC applications. A CEM II 52.5 N cement that contains between 6 and 20% limestone extender is employed. DuraPozz Class F fly ash, together with FerroAtlantica Microsilica silica fume, are used as rheology-modifying extenders. The locally mined Malmesbury fine aggregate used has a maximum particle size of 4.75 mm. A polycarboxylate ether superplasticizer, Chryso Premia 310, is added to aid with adequate workability and thixotropy.

4.2. Fresh state properties

The air content of the 3D printable material is determined before and

Fig. 5. Rectangular printed concrete section with 15 mm layer height from which 3DPC samples tested were cut.

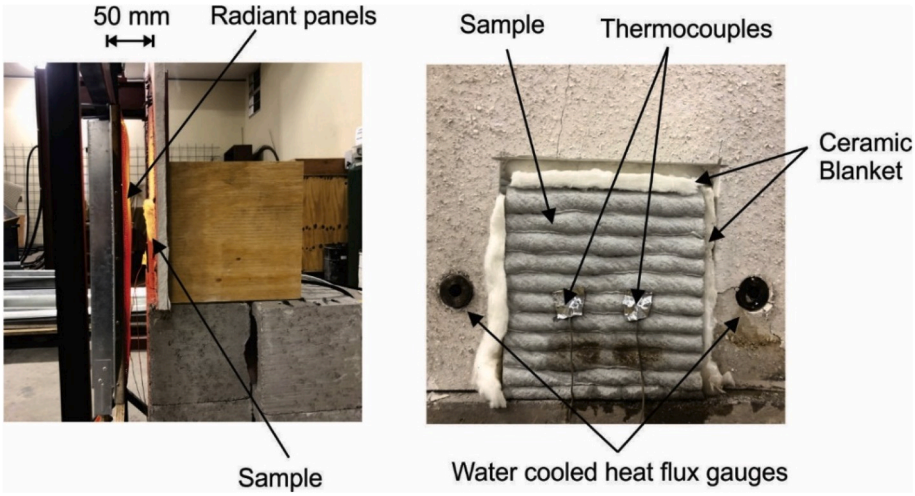

Fig. 6. Experimental setup showing the radiant panel setup and a 3DPC sample tested.

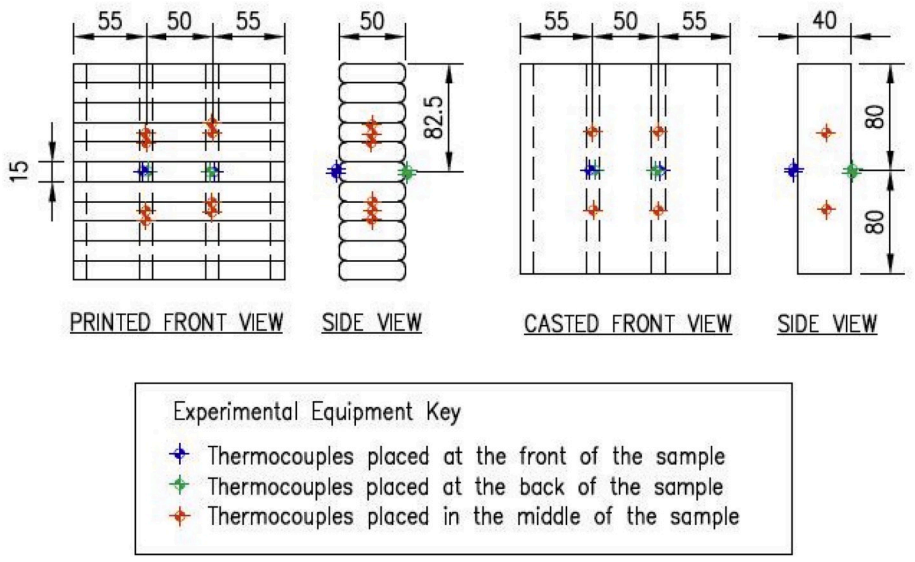

Fig. 7. Instrumentation layout. Printed layout (top left images), and casted layout (top right image). All units in mm.

Table 1
3DPC mix constituent quantities.

Constituent	Description	kg
Cement	PPC SureTech 52.5 N	579
Fly Ash	DuraPozz Class F	165
Silica Fume	SiliconSmelters Microfume	83
Fine Aggregate	Local Malmesbury	1167
Water	Potable Tap Water	261
Superplasticizer	Chryso Premia 310	5.75

after extrusion through the nozzle with the use of Forney's Press-Aire Meter [15]. The air meter is classified as type B and the test executed according to SANS 6252 [16]. The concrete density is also determined for both casted and pumped concrete by filling a known volume and obtaining the corresponding sample's mass. The results are presented in Table 2.

The results indicate that the extruded concrete has 0.9% less entrapped air than the casted concrete. The effect thereof is evident in the densities, where the extruded concrete is denser by 23 kg/ m^3.

Table 2
Air content and density of casted vs pumped concrete.

	Air Content (%)	Density (kg/m^3)
Casted (not pumped)	6	2061
Extruded (pumped)	5.1	2084

4.3. Hardened state properties

The 3D printable concrete's compressive and flexural strength is determined at 7 day curing age (i.e. the same day of testing). Three different configurations are tested, namely conventionally casted concrete samples in moulds (denoted NCC#), extruded/pumped concrete samples in moulds (denoted P#, i.e. formed using 3D printing extrusion within a contained space) and 3D printed samples denoted (3DP#). The compressive test moulds have dimensions 100 × 100 × 100 mm and follows the methodology depicted in SANS 5863 [17]. The flexural test moulds have dimensions 40 × 40 × 160 mm and follows the methodology set out in EN 196-1 [18]. The 3D printed flexural samples are saw-cut from a 3D printed element and tested in four point bending with interlayers aligned vertically, as depicted in Fig. 8. All specimens were

cured in a climate-controlled chamber at 23 °C and 65% relative humidity. The tests were performed in a Zwick Z250 material testing machine and 2 MN Contest cube press machine. The results are presented in Table 3.

The 3D printable concrete has a 7-day compressive strength of 41 MPa when casted, and slightly higher at 47.82 MPa when pumped. The approximate 28-day compressive strength can be extrapolated from the 7-day strength, assuming that concrete typically attains 70% of its 28-day strength at 7 days. Both the casted and pumped concrete possess compressive strengths larger than 50 MPa at 28-day curing age, which classifies it as a HPC [19]. It is clear that the reduced air content of the pumped concrete caused the increased compressive strength. The pumped concrete samples possess a 7-day flexural strength of 5.05 MPa, which is 0.84 MPa more than that of the casted samples. However, the 3D printed samples possess a flexural strength of 3.51 MPa, which is 1.53 MPa less than the pumped samples. Essentially, the pumping process increased the concrete's flexural strength by 19.87%, while the interlayer bond of the 3D printed samples (see Fig. 8) reduced the flexural strength by 30.38% compared to its bulk (pumped) concrete. Further work is required to understand the high variation in flexural strength compared to the low variation in compressive strength of the pumped concrete. It is postulated that the shape, size, interconnectedness and orientation of the voids in the concrete (see Fig. 9 and Fig. 10) influence internal micro crack propagation, whilst the degree thereof depends on the internal stress state induced by the load type.

4.4. Computed tomography scan of 3DPC interlayer

Figs. 9 and 10 depict the x-ray tomography (XRT) scans of the conventionally casted concrete samples and the 3DPC samples, respectively. X-ray Micro-computer tomography was performed at the Central analytical Facility of Stellenbosch University, and Volume Graphics VG Studio Max 3.3 was used to perform porosity and inclusion analysis. The samples in Figs. 9 and 10 were 20 × 20 × 20 mm in dimension (to give good resolution of smaller voids). Thus, Fig. 10 shows only one interlayer.

It should be noted that the scans only show voids larger than 1 mm in diameter in order to make the results more clear. Including smaller voids make it extremely difficult to obtain any useful information in this case. By comparing Figs. 9 to 10, it is clear that the 3DPC samples have a higher permeability and porosity compared to the conventionally casted concrete samples. Furthermore, from Fig. 10, it seems that the permeability is even higher between layers compared to within the layers themselves.

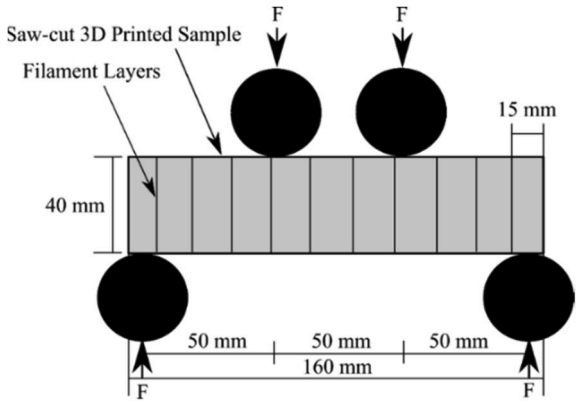

Fig. 8. Schematized four point bending test setup of a saw-cut 3D printed sample.

5. Results and discussion

This section is subdivided into the following four subsections: (a) results and discussion of the normal casted concrete (NCC) samples, (b) results and discussion of the 3DPC samples, (c) results and discussion of the cut 3DPC (C3DPC) samples, and (d) overarching discussion regarding the most significant differences between (a), (b) and (c). During some tests a technical problem was experienced with the gas supply to the panels which stopped operating for a few seconds several times during the test, resulting in a dip in the heat fluxes and associated cyclic heating, as seen in Figs. 11 and 16 and Fig. 23. It is most noticeable in Fig. 16 during the testing of sample 1. However, temperature results obtained are not affected and is still suitable for analyzing the behavior and failure mechanisms.

5.1. Conventionally casted concrete

Fig. 11 depicts the average heat fluxes emitted onto the two NCC samples, as measured by the HFGs. Fig. 12 and Fig. 13 depict the time-temperature curve inside the samples and surface temperatures of the samples, respectively.

Sample 1 and 2 spalled (thermo-hygral) at approximately 11.8 and 21.2 min, respectively. The time at which spalling occurred, corresponds with the peak front surface temperatures (Fig. 13) and peak temperatures inside the samples (Fig. 12). The aftermath of these two experiments are depicted in Fig. 14 and Fig. 15. Spalling is a function of various factors, but with previous research studies showing contrary results, the exact mechanisms causing the damage due to spalling is still incompletely understood [5]. Currently, a unified fire-induced concrete spalling theory [20] has been proposed to explain the seemingly contrary results that previous theories fail to explain. Fire-induced spalling can be categorized into three types according to their distinct governing mechanisms, thermo-hygral, thermo-mechanical and thermo-chemical spalling, with the spalling mentioned in this paper referring to thermo-hygral spalling (usually referred to as explosive spalling). Predicting the risk of spalling has widely been associated with concrete properties such as permeability, density, and strength [5,21]. Since the focus of this work is on 3DPC at elevated temperatures, the factors leading to spalling are not further discussed here. Although the problem seems extensive, spalling can generally be avoided by adding, for example, polypropylene (PP) fibres to the concrete mix. Once heated, the PP fibres begin to melt and as a result it increases the porosity, leaving cavities through which the water vapour can escape [5].

5.2. 3D printed concrete

Fig. 16 depicts the average heat fluxes emitted onto the 3DPC samples, as measured by the HFGs. Fig. 17 and Fig. 18 depict the time-temperature curve inside the center of the samples and the surface temperatures of the samples, respectively.

None of the 3DPC samples experienced thermo-hyral spalling during the experiments. Since the permeability of the 3DPC is apparently higher compared to the conventionally casted concrete (see Figs. 9 and 10), it allows vapour movement through the sample, reducing the pore pressure build up, which ultimately decrease the likelihood of spalling to occur [21]. All samples cracked during the course of the experiments. Unfortunately, since the samples were insulated with ceramic blanket on all sides, it was not possible to visually determine when the cracks occurred. After the experiments, the samples were left to cool down to ambient temperature. It is clear that all samples cracked along the interlayers and all three samples delaminated between layers when a mild force was applied by hand, as depicted in Fig. 19 to 21.

A possible explanation can be that the self-equilibrating tension stresses, induced as a result of the thermal gradient, exceeds the flexural capacity of 3.51 MPa of the printed samples. Fig. 22 plots the strains (total, thermal and mechanical) and mechanical stress in 3DPC Sample

Table 3
Compressive and flexural strength of casted, pumped and 3D printed concrete.

Specimens	Description	Force (N)	Stress – 7 day (MPa)	Stress – 7 day average (MPa)	Std. Dev (MPa)	CoV (%)	Stress - 28 day approx. (MPa)	Stress – 28 day average (MPa)
NCC1	4 Point Bending Test for Flexural Strength	1649.94	3.87	4.21	0.30	7.07	5.52	6.02
NCC2		1873.19	4.39				6.27	
NCC3		1866.81	4.38				6.25	
P1		2641.61	6.19	5.05	1.12	22.21	8.84	7.21
P2		2133.87	5.00				7.14	
P3		1685.66	3.95				5.64	
3DP1		1762.63	3.33	3.51	0.38	10.94	4.76	5.02
3DP2		1836.62	3.25				4.65	
3DP3		2036.06	3.96				5.65	
NCC1	Cube Test for Compressive Strength	385 835	38.58	41.08	2.50	6.09	55.11	58.69
NCC2		435 921	43.59				62.27	
NCC3		410 878	41.08				58.68	
P1		475 725	47.57	47.82	0.25	0.53	67.95	68.32
P2		480 815	48.08				68.68	
P3		478 270	47.82				68.31	

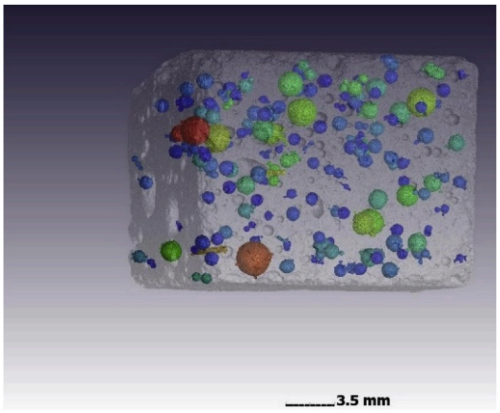

Fig. 9. X-ray tomography scan of the NCC.

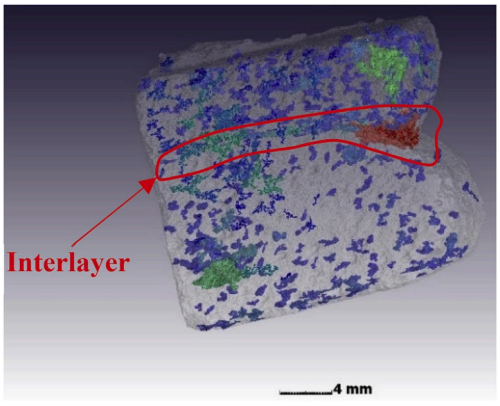

Fig. 10. X-ray tomography scan of the 3DPC. Contour indicate interconnected voids.

1 at 46 min. This has been calculated using [22] with material models being based upon EN 1992-1-2, with detailed explanations and a parametric study conducted in Ref. [23]. Further research is required to characterize elevated temperature-stress-strain behavior of 3DPC, but this calculation provides an estimate of stresses experienced. From the figure it can be observed that for approximately 7 mm on the exposed face and 10 mm on the unexposed face the sample experiences compression, whilst the central region is in tension. The maximum tensile stress is 2.5 MPa, where the actual reduced flexural stress of the sample is 2.1 MPa (using the 300 °C temperature at the point of

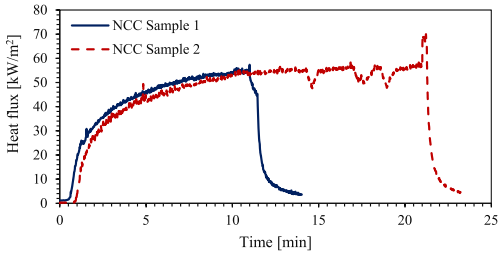

Fig. 11. Heat fluxes emitted onto the NCC samples.

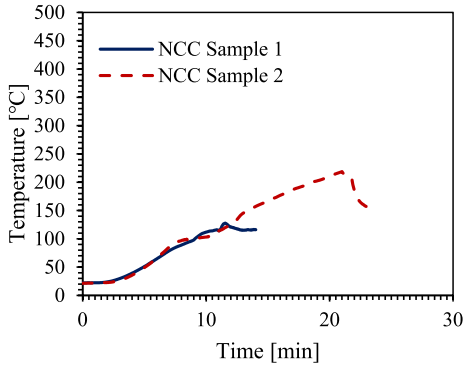

Fig. 12. Temperatures inside the center of the samples.

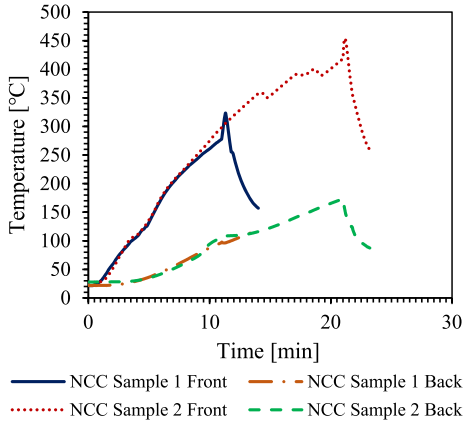

Fig. 13. Front and back surface temperatures.

Fig. 14. Aftermath of NCC sample 1.

Fig. 15. Aftermath of NCC sample 2.

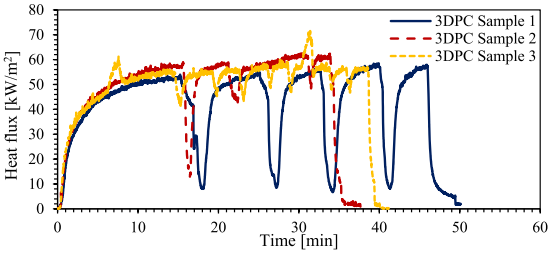

Fig. 16. Heat fluxes emitted onto the 3DPC samples.

maximum stress, and assuming flexural strength to reduce at the same rate as tensile stresses according to EN 1992-1-2). Hence, this indicates that the thermal forces induced at the interfacial zones are sufficient to cause failure, with failure likely to start in the middle of a section, rather than at the edges as might be expected. This indicates that reduced flexural stresses, as presented in Table 3, may contribute to cracking behavior, especially when reinforcement is not present.

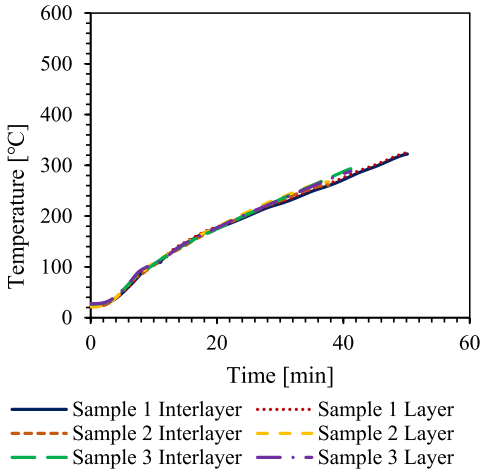

Fig. 17. Temperatures inside the center of the 3DPC samples.

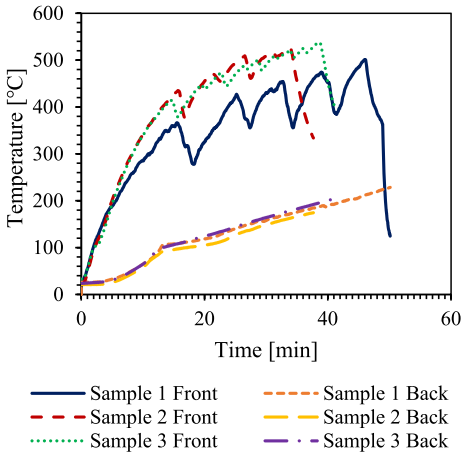

Fig. 18. 3DPC Front and back surface temperatures.

Fig. 19. 3DPC Sample 1 – Interlayer delamination.

5.3. Cut 3D printed concrete

Fig. 23 depicts the average heat fluxes emitted onto the C3DPC samples, as measured by the HFGs.

Fig. 20. 3DPC Sample 2 – Interlayer delamination.

Fig. 21. 3DPC Sample 3 – Interlayer delamination.

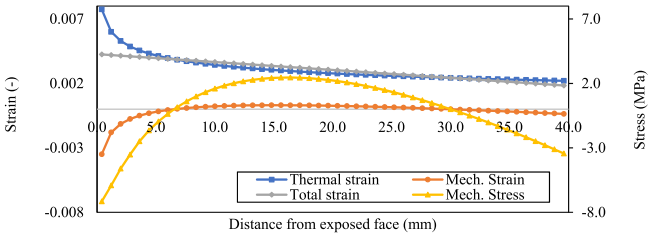

Fig. 22. Strains and mechanical stress in 3DPC Sample 1 at 46 min.

Fig. 24 and Fig. 25 depict the time-temperature curve in the center of the samples and the surface temperatures of the samples, respectively.

The C3DPC samples experienced the same delamination failure as the 3DPC samples, except for Sample 1 (Fig. 26) that experienced thermo-hygral spalling between layers. Spalling here was identified by loud popping noises at approximately 12 min into the experiment, at a heat flux of about 60 kW/m^2.

Samples 2 and 3 cracked during the course of the experiments, similar to the 3DPC samples. After the experiments, samples 2 and 3 were left to cool down to ambient temperature. It is clear that the samples cracked along the interlayers and both samples delaminated between layers under load applied by hand, as depicted in Fig. 27 and

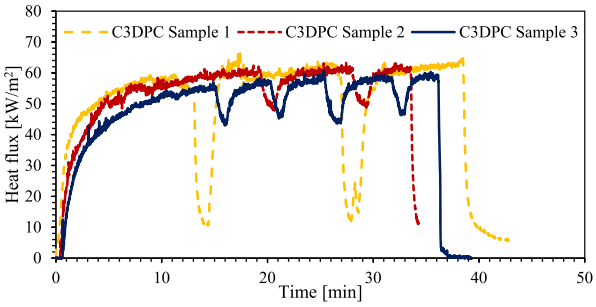

Fig. 23. Heat fluxes emitted onto the C3DPC samples.

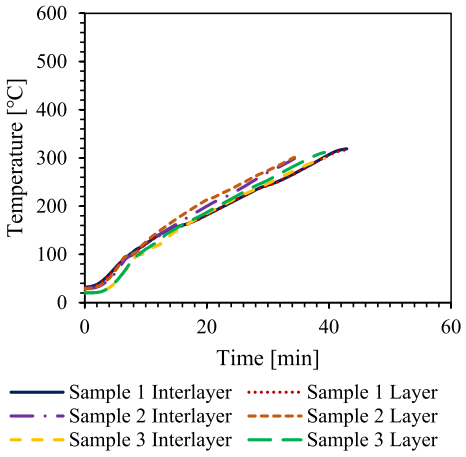

Fig. 24. Temperatures in the center of the C3DPC samples.

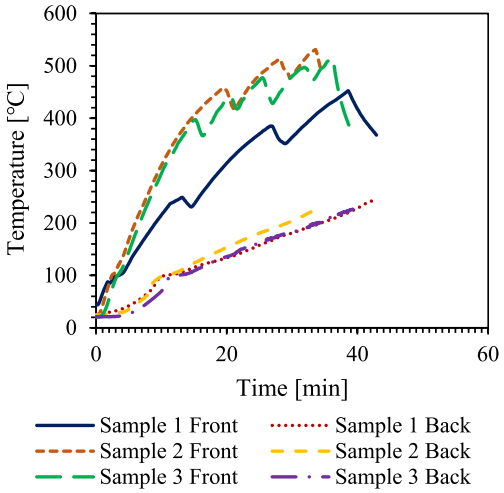

Fig. 25. C3DPC Front and back surface temperatures.

Fig. 28.

5.4. Discussion

A major concern regarding the 3DPC samples is the tendency of the interlayer bonds to break at elevated temperatures. For load bearing elements, interlayer cracks may result in stability failure, whereas for non-load bearing elements it will result in integrity failure. The addition of steel fibres to 3PDC mix, will possibly also not reduce the likelihood of delamination occurring since the fibres will generally be situated within the layers, and will not act as a bridge between layers. It is postulated

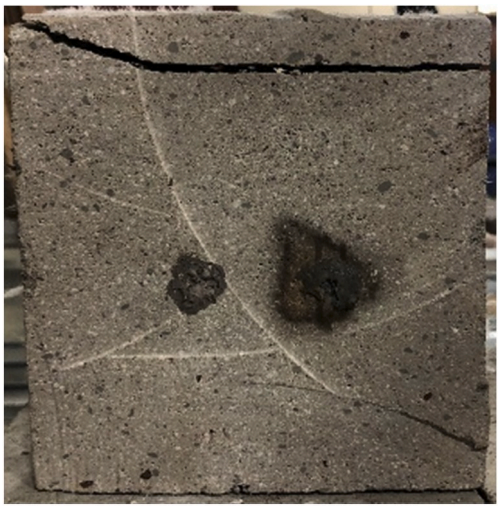

Fig. 26. C3DPC Sample 1 – Interlayer delamination as a result of spalling.

Fig. 27. C3DPC Sample 2 – Interlayer delamination.

Fig. 28. C3DPC Sample 3 – Interlayer delamination.

that the weakness formed between layers, as a result of higher porosity, is further weakened by the internal stresses due to the thermal gradient, highlighting a potential problem of the behavior of 3DPC in fire. In larger elements, and when structures are restrained, this problem may be reduced. Since spalling can be avoided by adding, for example, PP fibres to the concrete mix, it is not seen as a critical defect when comparing the 3DPC samples to the conventionally casted samples. In the isolated case where spalling occurred for the C3DPC sample, the behavior observed was different compared to the NCC samples. For this isolated C3DPC sample, the layers delaminated in a more explosive way, whereas for the NCC samples, spalling was significantly more destructive.

6. Conclusions

This paper presented a simple but novel experimental study looking at the behavior of 3DPC at elevated temperatures. The focus of this preliminary work has been on whether the process of forming 3DPC structures has an effect on its fire resistance and provides guidance for the way forward in terms of research needs regard 3DPC in fire. The main conclusions that can be drawn from this paper are as follows:

- The behavior of 3DPC, in general, has similar behavior to NCC and no specifically unusual behavior was observed.
- Failure occurred consistently at the interfaces for the 3DPC samples, indicating that the material strength is higher away from the interface. Interlayer bond failure occurred as a result of a thermal gradient that induced self-equilibrating tensile tresses, which were higher than the flexural resistance of the 3DPC samples expected at elevated temperatures. Hence, a study is required to characterize the elevated temperature performance of 3DPC under load, as limited data is currently available to understand what temperatures and stresses will cause failure;
- Air content is reduced in 3DPC compared with NCC (Table 2). Reduced air content increases compressive strength (20%), however 3DCP has lower flexural strength, as a result of the interlayer bonds (in this case it is 30% lower than NCC).
- Undulating surfaces of the 3DPC samples may influence the heat transfer into a section and may cause stress concentrations to occur. Further work is required to understand the influence of surface geometry on internal stresses and temperatures.
- As introduced above, since lamina are often placed individually and linked to other lamina in a truss-like manner, the behavior of individual lamina needs to be considered, as widths vary depending on the extrusion process and equipment used. The thickness of 3DPC lamina will severely influence the internal stresses generated when heated. It needs to be understood what minimum lamina thickness would be required, depending on the fire resistance required.
- The XRT scans showed that the 3DPC samples had higher void interconnectivity and higher associated permeability compared to the casted concrete, which reduced the likelihood of thermo-hygral spalling of the 3DPC samples. The XRT scans further showed that the interlayers had an even higher permeability compared to the layers, creating weak zones in the 3DPC samples.
- Samples exposed to direct radiation (plus a small amount of convection) led to consistent explosive spalling in NCC, consistent delamination in 3DPC with undulating surface finish, and spalling in one C3DPC specimen (also between layers) and delamination in two specimens.

Declaration of competing interest

The authors hereby acknowledge the financial contribution of the following organisations in the completion of this work: the Lloyd's Register Foundation under the "Fire Engineering Education for Africa" grant and the Department of Trade and Industry of South Africa under THRIP Research Grant TP14062772324.

None of these organisations have vested interests in the work and no conflicts of interest exist in the publication of this work.

Acknowledgements

The authors would like to acknowledge the financial support of the Lloyd's Register Foundation under the "Fire Engineering Education for Africa" grant GA 100093 and the Department of Trade and Industry of South Africa under THRIP Research Grant TP14062772324.

References

[1] S.C. Paul, G.P.A.G. van Zijl, M.J. Tan, I. Gibson, A review of 3D concrete printing systems and materials properties: current status and future research prospects, Rapid Prototyp. J. 24 (2017) 784–798, https://doi.org/10.1108/RPJ-09-2016-0154.

[2] V. Mechtcherine, J. Grafe, V.N. Nerella, E. Spaniol, M. Hertel, U. Füssel, 3D-printed steel reinforcement for digital concrete construction – manufacture, mechanical properties and bond behaviour, Construct. Build. Mater. 179 (2018) 125–137, https://doi.org/10.1016/j.conbuildmat.2018.05.202.

[3] R.J.M. Wolfs, F.P. Bos, T.A.M. Salet, Hardened properties of 3D printed concrete: the influence of process parameters on interlayer adhesion, Cement Concr. Res. 119 (2019) 132–140, https://doi.org/10.1016/j.cemconres.2019.02.017.

[4] T.T. Le, S.A. Austin, S. Lim, R.A. Buswell, R. Law, A.G.F. Gibb, T. Thorpe, Hardened properties of high-performance printing concrete, Cement Concr. Res. 42 (2012) 558–566, https://doi.org/10.1016/j.cemconres.2011.12.003.

[5] A.H. Buchanan, A.K. Abu, Structural Desing for Fire Safety, second ed., John Wiley & Sons, LTD, 2017.

[6] O. Arioz, Effects of elevated temperatures on properties of concrete, Fire Saf. J. 42 (2007) 516–522, https://doi.org/10.1016/j.firesaf.2007.01.003.

[7] E.H. El-Tayeb, S.E. El-Metwally, H.S. Askar, A.M. Yousef, Thermal analysis of reinforced concrete beams and frames, HBRC J. 13 (2017) 8–24, https://doi.org/10.1016/j.hbrcj.2015.02.001.

[8] S. Werner, A. Rogge, The effect of various fire-exposed surface dimensions on the spalling of concrete specimens, Fire Mater. 39 (2014) 545–556, https://doi.org/10.1002/fam.

[9] M. Bastami, A. Chaboki-Khiabani, M. Baghbadrani, M. Kordi, Performance of high strength concretes at elevated temperatures, Sci. Iran. 18 (2011) 1028–1036, https://doi.org/10.1016/j.scient.2011.09.001.

[10] P.J. Kruger, M. van den Heever, S. Cho, S. Zeranka, G. van Zijl, High-performance 3D printable concrete enhanced with nanomaterials, in: Proc. Int. Conf. Sustain. Mater. Syst. Struct. New Gener. Constr. Mater., RILEM Publications S.A.R.L., Rovinj, Croatia, 2019, pp. 533–540.

[11] J. Kruger, S. Zeranka, G.P.A.G. van Zijl, An ab initio approach for thixotropy characterisation of nanoparticle-infused 3D printable concrete, Construct. Build. Mater. 224 (2019) 372–386, https://doi.org/10.1016/j.conbuildmat.2019.07.078.

[12] J. van der Putten, G. de Schutter, K. van Tittelboom, The effect of print parameters on the (micro)structure of 3D printed cementitious materials, in: First RILEM Int. Conf. Concr. Digit. Fabr. - Digit. Concr. 2018, 2018, pp. 234–244, https://doi.org/10.1007/978-3-319-99519-9_22.

[13] J.G. Sanjayan, B. Nematollahi, M. Xia, T. Marchment, Effect of surface moisture on inter-layer strength of 3D printed concrete, Construct. Build. Mater. 172 (2018) 468–475, https://doi.org/10.1016/j.conbuildmat.2018.03.232.

[14] J. Van Der Putten, G. De Schutter, K. Van Tittelboom, Surface modification as a technique to improve inter-layer bonding strength in 3D printed cementitious materials, RILEM Tech. Lett. 4 (2019) 33–38, https://doi.org/10.21809/rilemtechlett.2019.84.

[15] Forney, Air Meter/Press-Aire Meter, 2019.

[16] SABS, SANS 6252 - Concrete Tests - Air Content of Freshly Mixed Concrete - Pressure Method, 1.1, SABS Standards Division, Pretoria, 2006.

[17] SABS, SANS 5863 - Concrete Tests - Compressive Strength of Hardened Concrete, 2.1, SABS Standards Division, Pretoria, 2006.

[18] EN 196-1, Cement - Determination of strength, Build. Mater. 10 - Test. Methods. (n. d.), 66–71.

[19] M.A. Rashid, M.A. Mansur, Considerations in producing high strength concrete, J. Civ. Eng. 37 (2009) 53–63.

[20] J.C. Liu, K.H. Tan, Y. Yao, A new perspective on nature of fire-induced spalling in concrete, Construct. Build. Mater. 184 (2018) 581–590.

[21] J. Bošnjak, J. Ožbolt, R. Hahn, Permeability measurement on high strength concrete without and with polypropylene fibers at elevated temperatures using a new test setup, Cement Concr. Res. (2013) 104–144.

[22] R.S. Walls, C. Viljoen, H. de Clercq, Analysis of structures in fire as simplified skeletal frames using a customised beam finite element, Fire Technol. (2018), https://doi.org/10.1007/s10694-018-0762-7.

[23] R. Walls, C. Viljoen, H. de Clercq, Parametric investigation into the cross-sectional stress-strain behaviour, stiffness and thermal forces of steel, concrete and composite beams exposed to fire, J. Struct. Fire Eng. 11 (1) (2019) 100–117. In Press.